Significance of High Resolution GHRSST on prediction of Indian Summer Monsoon

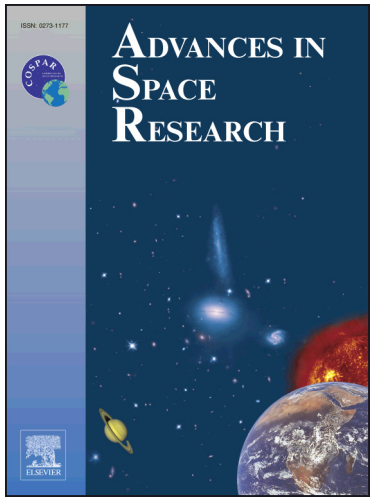

Significance of High Resolution GHRSST on prediction of Indian Summer Monsoon

Buddhi Prakash Jangid, Prashant Kumar, Attada Raju, Raj Kumar

PII: S0273-1177(17)30122-9
DOI: http://dx.doi.org/10.1016/j.asr.2017.02.025
Reference: JASR 13115

To appear in: *Advances in Space Research*

Received Date: 25 June 2016
Revised Date: 13 January 2017
Accepted Date: 15 February 2017

Please cite this article as: Jangid, B.P., Kumar, P., Raju, A., Kumar, R., Significance of High Resolution GHRSST on prediction of Indian Summer Monsoon, *Advances in Space Research* (2017), doi: http://dx.doi.org/10.1016/j.asr.2017.02.025

Significance of High Resolution GHRSST on prediction of Indian Summer Monsoon

Buddhi Prakash Jangid[1*], Prashant Kumar[1], Attada Raju[2] and Raj Kumar[1]

1. Atmospheric and Oceanic Sciences Group, EPSA, Space Applications Centre (ISRO), Ahmedabad, India
2. Physical Sciences and Engineering Division, King Abdullah University of Science and Technology (KAUST), Saudi Arabia

*Email- bp25physics@gmail.com,

Mobile. No. +91-8460332737

Abstract

In this study, the Weather Research and Forecasting (WRF) model was used to assess the importance of very high resolution sea surface temperature (SST) on seasonal rainfall prediction. Two different SST datasets available from the National Centers for Environmental Prediction (NCEP) global model analysis and merged satellite product from Group for High Resolution SST (GHRSST) are used as a lower boundary condition in the WRF model for the Indian Summer Monsoon (ISM) 2010. Before using NCEP SST and GHRSST for model simulation, an initial verification of NCEP SST and GHRSST are performed with buoy measurements. It is found that approximately 0.4 K root mean square difference (RMSD) in GHRSST and NCEP SST when compared with buoy observations available over the Indian Ocean during 01 May to 30 September 2010. Our analyses suggest that use of GHRSST as lower boundary conditions in the WRF model improve the low level temperature, moisture, wind speed and rainfall prediction over ISM region. Moreover, temporal evolution of surface parameters such as temperature, moisture and wind speed forecasts associated with monsoon is also improved with GHRSST forcing as a lower boundary condition. Interestingly, rainfall prediction is improved with the use of GHRSST over the Western Ghats, which mostly not simulated in the NCEP SST based experiment.

Key words: Indian Summer Monsoon, Sea Surface Temperature, WRF model, Seasonal Prediction

1. Introduction

The sea surface temperature (SST), which contains the information of moisture and energy through thermodynamic processes, is one of the important inputs for numerical weather prediction (NWP) models (Nayak, 2006, Shetye et al., 1996). SST plays an important role in the formation of sea breezes, air-sea interaction processes, and also one of the major parameters that causes natural disasters like tropical cyclone (Palmen, 1948, Miller, 1958, Uma and Selvaraj, 2012, Kumar et al., 1999, Gadgil et al., 1984). Zhang et al. (2002) found large influence of winter and spring equatorial Indian ocean SST on the Indian summer monsoon (ISM) rainfall, which showed that SST has ample potential as a predictor for the ISM rainfall prediction. Traditionally, SST is measured by buoy/ship at different depths, which are very sparse over Indian region. Space-borne passive infrared and microwave sensors are used frequently to retrieve SST over globe (Minnett et al., 2002, Guan et al., 2003, Shahi et al., 2011). The SST retrieve from satellite has a large coverage, but it measures skin SST only (at micrometer level) whereas, *in situ* (like buoy, ship) measures bulk SST. These two SST are differing significantly under weak winds and strong solar insolation (Fairall et al., 1996, Wick et al., 1996, Zeng et al., 1999).

Various sensitivity studies (Messager et al., 2004, Rao et al., 2004, Cuadra and Da Rocha, 2007, Chowdary et al., 2014) have been performed to assess the impact of SST on regional climate prediction. Messager et al. (2004) used regional climate model (RCM) to assess the impact of regional SST on rainfall prediction during drought period of the West African monsoon and showed that RCM is able to capture the deficit rainfall over this region. Cuadra and Rocha (2007) evaluated the impact of SST over the South Atlantic Ocean on the inter-annual variability

of the simulated precipitation and air temperature using RegCM3 model. They found that if persistent SST is warmer (colder) than the observed SST, the seasonal precipitation increases (decreases). Moreover, Marengo et al. (2003) showed that the global circulation model (GCM) with observed SST properly simulated the accompanying rainfall anomalies in many regions of the world, and the skill dropped in absence of anomalies. Chowdary et al. (2014) demonstrated that the monsoon rainfall over South Asia was mostly determined by the Indian Ocean SST during summer 2010. Raju et al. (2014) studied ISM 2010 using Weather Research and Forecasting (WRF) model with prescribed SST, and they reported that model has overestimated rainfall over Indian region. Lei et al. (2008) studied historical Mumbai heavy rainfall using an explicit urban energy balance model to simulate the Mumbai urban heat island and the TRMM prescribed sea surface temperature (SST) fields in the Regional Atmospheric Modeling System (RAMS). They found that this heavy rainfall event was a result of a stationary convergence zone caused by SST gradients just off Mumbai and the sensible-heat flux gradients due to the urban heating over Mumbai (Kumar et al., 2008). Samala et al. (2013) used the Weather Research and Forecasting model and the Regional Ocean Modeling System (ROMS), with an attempt to address the issue of air–sea interactions in the simulation of the Indian Summer Monsoon rainfall, circulations, sea surface temperature (SST) and the intra-seasonal variability.

In case of short-range weather forecast, Case et al. (2007) suggested that SST product from Moderate Resolution Imaging Spectroradiometer (MODIS) satellite in regional weather forecast models have a significant positive impact on prediction (Case et al., 2007). Authors found that more accurate specification of the lower-boundary forcing within the WRF model resulted in improved land/sea fluxes and hence, more accurate evolution of coastal mesoscale circulations

and the associated sensible weather elements. The use of high resolution MODIS SST composite to initialize the Advanced Research WRF model has been shown potential to improve the prediction of sensible weather parameters in coastal regions (LaCasse et al., 2008). Yamamoto and Hirose (2009) examined the influence of high-resolution SST obtained from an ocean assimilation model on simulated monthly precipitation and found that the assimilation of SST data leads to improved regional atmospheric simulations of monthly precipitation. They have used high and low resolution SST analysis products in the WRF model for May 2004 for short-term forecasts over Florida and surrounding waters. The impact of using a 1 km MODIS SST composite on subsequent evolution of the marine atmospheric boundary layer is assessed through simulation comparisons and limited validation (LaCasse et al., 2008). Rao et al. (2004) showed the importance of real SST on ISM prediction when MM5 model was initialized from National Centers for Environmental Prediction (NCEP) reanalysis. Therefore, accurate representation of SST as lower boundary condition from high resolution observations is necessary for ISM prediction from regional models.

The Group for High Resolution SST (GHRSST) is a merged high temporal and spatial resolution SST product which used multi-satellite derived SST for gaining better understanding of the ocean-atmosphere interaction (Kim et al., 2011). The objective of the GHRSST is to provide the best quality SST product for various scientific applications in short to long time scales. In this study, two simultaneous experiments are performed using Advanced Research WRF (ARW) model to assess the impact of SST, a slow varying boundary condition, from GHRSST on ISM prediction during year 2010.

2. GHRSST Data

The GHRSST was set up to promote an International collaboration for development of new global, multi-sensor, high resolution near real time SST products (http://podaac.jpl.nasa.gov/GHRSST/). The aim of this project is to make available the best quality SST for various scientific applications in different time scales. Operational SST data product at a spatial resolution of 1 km is available from GHRSST. The input SST data include infrared (IR) sensors (e.g., AVHRR, METOP, MODIS, AATSR) with a spatial resolution of 1 km, the Geostationary Satellites (GOES, MTSAT, SEVIRI/MSG) with a spatial resolution of 5 km, and microwave sensors (e.g., AMSR-E, TMI) with a spatial resolution of 25 km. The *in-situ* SST measurements from ships, moorings, surface drifters, and profiling floats are also used. Each instrument has its own strengths and weaknesses depending on the sensor type, platform, orbit and so on. With the objective of producing accurate SST data at highest possible spatial resolution over globe, various sources of SST data are combined in the GHRSST .

2.1 Comparison of GHRSST with Buoy over Indian region

Temporal variation of SST from Buoy, NCEP global model analysis and GHRSST during 01 May to 30 September 2010 is shown in Figure 1. It is observed that NCEP and GHRSST shows the seasonal evolution of SST with higher SST during May (transition period) and lower SSTs during rest of monsoon phase as in buoy observations. The NCEP analyzed SST is smooth, whereas, GHRSST is able to capture the variations of SST very nicely during this period (Fig. 1). Maximum difference between Buoy and GHRSST is ~ 1 K during this period. Six buoy observations available over the Indian Ocean are used to validate the GHRSST and NCEP SST. Initial verification shows that approximately 0.3 to 0.4 K root mean square

difference (RMSD) in the GHRSST and NCEP SST respectively during this period with very less bias (~0.1 K) in both SST data. GHRSST is much closer to buoy measurements as compared to NCEP SST. These initial results show that GHRSST has sufficient potential for weather modeling applications. In general, global model (here NCEP) SST available at coarse resolution, which is used as lower boundary conditions for regional model. In this study, a high resolution GHRSST is used as lower boundary condition to assess the impact of finer resolution SST compared to coarse resolution SST from global model.

3. Model and experimental design

The Weather Research and Forecasting model (Skamarock and Klemp, 2008) version 3.4 mainly developed for operational and research application is used in this study to assess the impact of high resolution GHRSST on seasonal prediction of ISM 2010. The WRF model includes advance numerical techniques, nesting options and various physics options for the treatment of convection and precipitation. This version utilizes Arakawa C-grid staggering for the horizontal grid and a fully compressible system of equations; a terrain-following hydrostatic pressure coordinates with stretched vertical grid is imposed vertically. The time-split integration uses a third-order Runge-Kutta scheme (Wicker and Skamarock, 2002) with a smaller time step for acoustic and gravity wave modes. The physics options of WRF model consist of the single moment 6-class simple ice scheme for microphysics (Lin et al., 1983); the Kain–Fritsch scheme (Kain, 2004) for the cumulus convection parameterization, and the Yonsei University planetary boundary-layer scheme (Hong and Dudhia, 2003). For long wave and shortwave radiation the Rapid Radiative Transfer Model (RRTM) (Mlawer et al., 1997) and the Dudhia scheme (Dudhia, 1989) are used respectively. In this version of the WRF model, the Noah land-surface model

(Chen and Dudhia, 2001), which contains four soil layers namely 0–0.1, 0.1–0.4, 0.4–1.0, and 1.0–2.0 m below the surface is selected. The model configuration has given in Table 1. Topography as well as snow cover information are obtained from United States Geological Survey.

Table 1: A summary of Characteristics of the WRF model

S. No.	Characteristic Feature	Scheme
1	Horizontal grid	Arakawa C grid
2	Map projection	Mercator
3	Time integration scheme	Third-order Runge–Kutta (Wicker 2002)
4	Dynamics	Non-hydrostatic with 3D Coriolis force
4	Microphysics	WSM 6-class graupel scheme (Lin 1983 and Dudhia 2008)
5	Short wave Radiation	Dudhia scheme (Hong 2004)
6	Long wave Radiation	RRTM scheme (Mlawer 1997)
7	Land Surface physics	Unified Noah land-surface model (Chen 2001)
8	PBL physics scheme	YSU (Hong 2006)
9	Cumulus parameterization scheme	Kain-Fritsch scheme (Kain 1990, Kain 1993 and Kain 2004)
10	Lateral boundary conditions	NCEP GDAS
11	Lower boundary condition	NCEP and GHRSST
12	Initial conditions	NCEP GDAS

The WRF model is customized here for seasonal prediction in which SST information is used as lower boundary conditions, and lateral boundary conditions are taken from NCEP Global Data Assimilation System (GDAS) analysis at $1^\circ \times 1^\circ$ spatial resolution. Two different SST data available from NCEP GDAS and GHRSST are used to assess the impact of high resolution SST

against low resolution SST on regional model simulations over Indian region. Two experiments named as CNT (with NCEP SST) and GSE (with GHRSST) are performed using SST from NCEP and GHRSST respectively. Both the experiments are initialized from 0000 UTC 01 May 2010 for prediction up to 0000 UTC 30 September 2010. Six hourly NCEP analyses at $1°\times1°$ spatial resolution is used to generate the lateral boundary conditions. The WRF model has a spatial resolution of 30 km with 310×310 number of grid points with longitude from $38.5\,°$ E to $121.5\,°$ E and latitude from $38.3\,°$ S to $38.3\,°$ N.

4. Results and Discussions

For statistical evaluation of the WRF model predictions, bias and RMSD are considered. A forecast impact parameter is defined using RMSD of CNT and GSE experiments.

$$RMSD = \sqrt{\frac{\sum_{i=1}^{N}(F_i - O_i)^2}{N}} \tag{1}$$

$$FI = \sqrt{\frac{\sum_{i=1}^{N}(C_i - O_i)^2}{N}} - \sqrt{\frac{\sum_{i=1}^{N}(G_i - O_i)^2}{N}} \tag{2}$$

In equation (1), '*F*' is defined as forecast from CNT (*C*) and GSE (*G*) experiments. '*O*' is represented as truth value. The NCEP final analysis is considered as truth for temperature, moisture and winds. Rainfall predictions are compared with TRMM 3B42 merged rainfall product (Kumar et al., 2016). Total numbers of forecasts are denoted by '*N*'. In equation (2), a positive (negative) value of forecast impact (FI) shows improvement (degradation) in the WRF model forecasts for GSE experiments compared to CNT experiments. FI near to zero represents neutral impact on model predictions.

4.1. Temperature

Spatial distribution of mean low level (at 850 hPa) temperature analysis from the NCEP data is shown in Figure 2(a). Mean temperature analysis represents high temperature over the Iran, Saudi Arabia and Iraq region, and low temperature over the Indian landmass. Slightly higher temperature can be seen over the north-western part of India mainly over the desert of Rajasthan. Overall, it is observed that high temperatures over the Indian subcontinent region and lower temperatures over oceanic region. It shows the meridional temperature gradient between land and sea, which is one of the important factors for monsoon establishment. Apart from that, higher temperature (thermal low) can be seen over north-western part of India mainly over the desert of Rajasthan, and it extends up to Iran, Saudi Arabia and Iraq region. RMSD in low level temperature forecasts from CNT experiments (Fig. 2b) show that less than 3 °C error over the oceanic region except head Arabian Sea (AS). Slightly larger error can be seen over the Saudi Arabia, Gangetic plains and Himalayan foothills. This large error in CNT experiments reduced with the use of high resolution SST forcing from GHRSST (Fig. 2c). It is important to note that forecasts from GSE experiment are improved over the head AS and nearby coastal regions. These results indicate that finer resolution SST has more positive impact when SST variations are large, while coarser resolution SST from NCEP analysis are not able to capture these variations. Figure 2(d) illustrates the spatial distribution of FI for low level temperature for GSE experiments compared to CNT experiments during ISM 2010. It shows that the low level temperature shows large positive impact over the Indian landmass and nearby coastal regions and Indian Ocean. Few pockets of small degradations are also seen over the Malaysia region. In

brief, Figure 2(d) shows that temperature prediction is improved largely after incorporating finer resolution SST over the south Asia region during monsoon season.

4.2. Water vapor mixing ratio

Spatial distribution of low level (850 hPa) mean water vapor mixing ratio (WVMR) from the NCEP final analysis during 01 June to 30 September 2010, RMSD (eq. 1) in CNT and GSE experiments when compared with the NCEP final analysis, and forecast impact (eq. 2) in WVMR at 850 hPa is shown in Figure 3. The mean value of the NCEP analysis shows maximum moisture (~16 g kg^{-1}) over the north-east region of India and Nepal (Fig. 3a). The AS adjacent to the southern peninsular India, Bay of Bengal (BoB) and Indian landmass have slightly more low level moisture compared to the equatorial Indian Ocean. RMSD in WVMR forecasts from CNT (Fig. 3b) and GSE (Fig. 3c) experiments shows higher error over the north and north-west part of India, head of AS, and Gulf of Oman regions. Slightly less RMSD is seen over the northern India in GSE experiments (Fig. 3c) compared to CNT experiments (Fig. 3b). Spatial distribution of forecast impact (Fig. 3d) shows that use of GHRSST improved largely the low level moisture forecast associated with monsoon over the Indian region and Gulf of Aden during ISM 2010 which shows the importance of high resolution SST on monsoon prediction. Few pockets of negative changes are found over the AS, equatorial Indian Ocean and some part of Malaysia, whereas, domain average value of forecast impact is positive. Overall, we found that use of high resolution SST improved the monsoon flow (due to proper thermal gradient between land and ocean), which in turn enhances the moisture supply over Indian land region during ISM 2010.

4.3. Winds

Spatial distribution of mean surface (at 10 m) wind speed from the NCEP final analysis valid for June to September 2010 period is shown in Figure 4. It shows that the NCEP final analyses are able to capture the mean monsoon low level circulation. More than 10 ms^{-1} surface wind speed is observed over the AS during monsoon season (Fig. 4a). RMSD in surface wind speed for CNT and GSE experiments are shown in Figure 4(b) and Figure 4(c) respectively. A RMSD of less than 4 ms^{-1} is found over most part of the study domain, particularly, over the equatorial Indian Ocean. It is also noted that less RMSD is seen over land except orographic regions where large error is observed. These large errors over orographic regions shows that the WRF model is not able to capture orographic induced forces precisely. This might be due to the improper interaction between land surface and atmosphere as this region is important heat source region during monsoon. Resolving these processes is great challenge in regional model as it strongly attributed to land surface models. Few pockets of large errors are also seen over the west coast of southern peninsular India, head BoB and Gulf of Aden regions. It is interesting to note here that use of GHRSST in the WRF model shows slightly less error over the AS and west coast of India, whereas small degradation is seen over the BoB region. Figure 4(d) shows the spatial distribution of FI, which clearly shows the large positive improvement over the AS, which shows that finer resolution of SST improved the near surface winds where winds have larger variability mainly over this region during summer monsoon. Moreover, negligible changes are found over the land regions. Few pockets particularly over the peninsular region and large part of the BoB have no improvement. This might be due to model response to the SST. It is important to examine this issue while using regional coupled model as it is resolves ocean feedback to atmosphere.

4.4. Temporal variation of Surface parameters

The temporal evolution of important surface parameters such as temperature, relative humidity, and wind speed during 01 June 2010 to 30 September 2010 over entire domain available from NCEP final analysis, CNT and GSE experiments are shown in Figure 5. Maximum difference between WRF model simulated temperature, moisture and wind speed with NCEP final analysis are ~1 K, 3 %, and 1 ms^{-1} respectively. Domain average value of temperature (Figure 5a) signifies decreasing trend in temperature from June to August, beyond that it shows almost constant variation. Seasonal predictions from the WRF model are able to capture this broad seasonal behavior with a warm bias in model prediction. It is important to discuss here that with the use of GHRSST forcing, mean temperature forecasts are improved marginally and is more close towards NCEP final analysis. However, no noteworthy changes are found beyond 01 August 2010. Similar to mean temperature variation, variation of domain average value of relative humidity (Fig. 5b) also shows that with GHRSST marginal improvement are seen in moisture prediction. Model is able to capture the increasing trend of moisture change, which matches well with NCEP final analysis. Moreover, small degradation can be seen in moisture prediction initially for few days. This small error in moisture may be due to chaotic behavior of moisture as compared to temperature that required more time for model spin up. Wind speed (Fig. 5c) predictions from the WRF model are able to capture the mean trend of surface wind speed during monsoon period. Slightly higher wind speed is available from GSE experiments matches with NCEP final analysis that underestimate from CNT experiments. Overall, we found that incorporation of finer resolution SST improved the surface parameters, which further help to improve other important model parameter like rainfall.

4.5. Rainfall

Spatial distribution of daily mean monsoon rainfall from TRMM 3B42 merged-rainfall product, CNT and GSE predictions during 01 June to 30 September is shown in Figure 6. Figure 6a shows that the maximum rainfall is observed over the west coast of southern peninsular India and northeastern part of India. However, less rainfall can be seen over the north-west India, central India and rain-shadow region of south-east India. The WRF model predicted mean monsoon rainfall from CNT experiments (Figure 6b) is not able to capture the high rainfall over the Western Ghats, and fails to predict rainfall over the northwestern part of India. However, CNT experiment is able to pick up rainfall over north-east India and central India. High rainfall is predicted by model over the equatorial Indian Ocean, which is not observed by TRMM rainfall. In brief, the WRF model is not able to capture mean monsoon characteristics during monsoon season when SST forcing is opted from NCEP SST. GSE (Fig. 6c) is able to capture the maximum rainfall zone over the Western Ghats which misses in CNT experiments. It is important to note that the GSE captures the finer details of orographic precipitation along the Himalayan foothills and Northeastern regions of India. Both model experiments are same, except change in SST forcing. So, these substantial improvements in rainfall prediction over this region is mainly due to high resolution SST information which improve model predicted low level temperature, winds and moisture and further improves the rainfall prediction. Similar kind of improvement in rainfall pattern (Fig. 6d) can also be seen over central India, equatorial Indian Ocean, AS and southern Indian Ocean. Few pockets of degradation can also be seen over the Indian landmass and BoB. In brief, Figure 6 shows that rainfall prediction is improved largely after incorporating finer resolution SST over the south Asia region during monsoon period. For

more detail description of forecast impact in rainfall prediction, we are selecting four monsoon core regions, based on the physical processes associated with local precipitation, viz. Western Ghats (72° E–77° E and 10° N–19°N), Central India (69° E–88° E and 18° N–28°N), Equatorial Indian Ocean (75° E–95° E and 5° S–5° N) and Head BoB regions (85° E–96° E and 17° N–24° N). Spatial distribution of $abs(C - T) - abs(G - T)$ is shown in Figure 7, which shows that positive value of parameter represents improve rainfall forecasts. Here, C, G and T represent daily rainfall from CNT, GSE, TRMM respectively. It shows a large improvement over the Western Ghats region. These large improvements are mainly due to positive impact in atmospheric winds, which subsequently improve the rainfall prediction over this region. Similar kind of positive impact in rainfall prediction can be seen over the Central India and equatorial Indian Ocean. Over the head of BoB, less than 15 mm day^{-1} rainfall is found except coastal region. CNT experiment shows slightly higher rainfall compared to TRMM and GSE estimated rainfall over northeast India. This region shows maximum improvement after incorporating GHRSST. Rainfall prediction is improved overall except near coastal region in head of BoB. Domain average value of improvement is always positive which represents that GHRSST improved the seasonal rainfall prediction skill of WRF model.

Moreover, we also computed statistical skill scores (Kumar et al., 2016) mainly bias score (BS) and equitable threat scores (ETSs) for 24 h accumulated rainfall which provides the skill of the WRF model to predict the frequency of rainfall occurrence events at or above a particular rainfall threshold. ETS and BS based on contingency table (Table 2) are computed over a wide range of rainfall thresholds.

$$ETS = \frac{(a - e)}{(a+b+c-e)} \ , where \ \ e = \frac{(a+b).(a+c)}{a+b+c+d} \quad (3)$$

$$BS = \frac{(a+b)}{(a+c)} \quad (4)$$

Here "*e*" refers to the expected number of correct forecasts above a rain threshold with a random forecast. Higher value of ETS represents better predictive skill, and BS is good when it is near to 1.

Table 2: Schematic 2 x 2 contingency table for the definition of scores.

	Observation ≥ Threshold	Observation < Threshold
Forecast ≥ Threshold	*a*=Hits	*b*=False alarms
Forecast < Threshold	*c*= Misses	*d*=Correct rejections

These scores are obtained by comparing 122 samples daily rainfall. After using GHRSST, the WRF model shows higher value of ETS and less bias score, which represents that skill of rainfall prediction is improved (Fig. 7). Bias score value shows positive bias (more than 1) for less rainfall thresholds and negative bias (less than 1) for larger rainfall thresholds in CNT, which indicate that CNT experiments over-estimated rainfall for less rainfall thresholds and underestimated the rainfall for extreme rainfall events. This discrepancy has improved with the implementation of GHRSST in the WRF model as it represents the accurate SST that leads to the proper zonal gradients and regulates the moist winds towards the land region.

5. Conclusions

In this study, high resolution SST available from GHRSST are used to assess the impact of SST, to improve lower boundary conditions of the NWP model, on seasonal monsoon forecast over Indian region. After initial verification of GHRSST with buoy observations, the SST data from GHRSST is used in the WRF model. The SST from NCEP is also used to inter-compare the performance of two different source of SST. Incorporation of high resolution SST improves the temperature, moisture, wind speed and rainfall forecasts. Our analysis show that large improvements are observed over the Indian landmass as well as AS and equatorial Indian Ocean in low level temperature, moisture and rainfall forecast after using finer resolution SST as lower boundary condition. Negligible changes are seen in wind speed forecast over Indian landmass but large positive improvements are found over the Arabian Sea as well as southern Indian Ocean. Temporal variations of surface parameters show large differences between WRF model simulated temperature (1 K), moisture (3 %) and wind speed (1 ms^{-1}) with NCEP final analysis. Results of temporal variation show that incorporation of finer resolution SST improved the surface temperature, wind speed and moisture. Higher value of ETS and less bias score are found in 24 hour accumulated rainfall by comparing 122 samples daily accumulated rainfall, which represents the improvement in skill of rainfall prediction. Overall, utilization of high resolution SST in WRF model improves the seasonal forecast.

Acknowledgements

The authors would like to thank Director, SAC. Authors are also thankful to Dr. Neeraj Agarwal for his motivation to use GHRSST in WRF model. Authors are thankful to NCAR for WRF model. The NCEP global model analyses are obtained from Data Support Section of the Computational and Information Systems Laboratory (CISL) at NCAR. TRMM data are obtained from http://daac.gsfc.nasa.gov/data/datasets. Authors are also thankful to Tropical Atmosphere Ocean project office of NOAA/PMEL to provide RAMA (Research Moored Array for African-Asian-Australian Monsson Analysis and Prediction) Buoy observations. www.pmel.noaa.gov/tao/data_deliv/deliv-nojava-rama.html.

References:

Case, J. L., LaCasse, K. M., Dembek, S. R., Santos, P. Lapenta, W. M. 2007. Impact of MODIS High-Resolution Sea-Surface Temperatures on WRF Forecasts at NWS Miami, FL.

Chen, F. Dudhia, J. 2001. Coupling an advanced land surface-hydrology model with the Penn State-NCAR MM5 modeling system. Part I: Model implementation and sensitivity. *Monthly Weather Review,* 129**,** 569-585.

Chowdary, J. S., Attada, R., Lee, J. Y., Kosaka, Y., Ha, K. J., Luo, J. J., Gnanaseelan, C., Parekh, A. Lee, D. Y. 2014. Seasonal prediction of distinct climate anomalies in summer 2010 over the tropical Indian Ocean and South Asia. *Journal of Meteorological Society, Japan,* 92**,** 1-16.

Cuadra, S. V. Da Rocha, R. P. 2007. Sensitivity of regional climatic simulation over Southeastern South America to SST specification during austral summer. *International journal of climatology,* 27**,** 793-804.

Donlon, C., Robinson, I., Casey, K. Vazquez-Cuervo, J. 2007. The global ocean data assimilation experiment high-resolution sea surface temperature pilot project. *Bulletin of the American Meteorological Society,* 88**,** 1197.

Dudhia, J. 1989. Numerical study of convection observed during the winter monsoon experiment using a mesoscale two-dimensional model. *Journal of the Atmospheric Sciences,* 46**,** 3077-3107.

Dudhia, J., Hong, S.-Y. Lim, K.-S. 2008. A new method for representing mixed-phase particle fall speeds in bulk microphysics parameterizations. *Journal of the Meteorological Society of Japan,* 86**,** 33-44.

Fairall, C. W., Bradley, E. F., Godfrey, J. S., Wick, G. A., Edson, J. B. Young, G. S. 1996. The cool skin and the warm layer in bulk flux calculations. *Journal of Geophysical Research,* 101**,** 1295-1308.

Gadgil, S., Joshi, N. Joseph, P. 1984. Ocean-atmosphere coupling over monsoon regions. *Nature,* 312**,** 141-143.

Guan, L., Kawamura, H. Murakami, H. 2003. Retrieval of sea surface temperature from TRMM VIRS. *Journal of oceanography,* 59**,** 245-249.

Hong, S. Y., Dudhia, J. Chen, S. H. 2004. A revised approach to ice microphysical processes for the bulk parameterization of clouds and precipitation. *Monthly Weather Review,* 132**,** 103-120.

Hong, S. Y., Noh, Y. Dudhia, J. 2006. A New Vertical Diffusion Package with an Explicit Treatment of Entrainment Processes. *Monthly Weather Review,* 134**,** 2318-2341.

Hong, S. Y. Dudhia, J. 17.3 Testing of a new nonlocal boundary layer vertical diffusion scheme in numerical weather prediction applications. 20th Conference on Weather Analysis and Forecasting, 2003 USA.

Kain, J. S. Fritsch, J. M. 1990. A one-dimensional entraining/detraining plume model and its application in convective parameterization. *Journal of the Atmospheric Sciences,* 47**,** 2784-2802.

Kain, J. S. Fritsch, J. M. 1993. Convective parameterization for mesoscale models: The Kain-Fritsch scheme. *The representation of cumulus convection in numerical models.* Springer.

Kain, J. S. 2004. The Kain-Fritsch convective parameterization: An update. *Journal of Applied Meteorology*.

Kim, M. J., Ou, M. L., Sohn, E. H. Kim, Y. 2011. Characteristics of sea surface temperature retrieved from MTSAT-1R and in-situ data. *Asia-Pacific Journal of Atmospheric Sciences,* 47**,** 421-427.

Kumar, A., Dudhia, J., Rotunno, R., Niyogi, D. Mohanty, U. 2008. Analysis of the 26 July 2005 heavy rain event over Mumbai, India using the Weather Research and Forecasting (WRF) model. *Quarterly Journal of the Royal Meteorological Society,* 134**,** 1897-1910.

Kumar, K. K., Rajagopalan, B. Cane, M. A. 1999. On the weakening relationship between the Indian monsoon and ENSO. *Science,* 284**,** 2156-2159.

Kumar, P., Bhattacharya, B. K. Pal, P. 2015. Evaluation of Weather Research and Forecasting Model Predictions Using Micrometeorological Tower Observations. *Boundary-Layer Meteorology,* 157**,** 293-308.

Kumar, P., Kishtawal, C. Pal, P. 2016. Skill of regional and global model forecast over Indian region. *Theoretical and Applied Climatology,* 123**,** 629-636.

LaCasse, K. M., Splitt, M. E., Lazarus, S. M. Lapenta, W. M. 2008. The impact of high-resolution sea surface temperatures on the simulated nocturnal Florida marine boundary layer. *Monthly Weather Review,* 136**,** 1349-1372.

Lei, M., Niyogi, D., Kishtawal, C., Pielke Sr, R., BeltrĂĄn-Przekurat, A., Nobis, T. Vaidya, S. 2008. Effect of explicit urban land surface representation on the simulation of the 26 July 2005 heavy rain event over Mumbai, India. *Atmospheric Chemistry and Physics,* 8**,** 5975-5995.

Lin, Y. L., Farley, R. D. Orville, H. D. 1983. Bulk parameterization of the snow field in a cloud model. *Journal of Climate and Applied Meteorology,* 22**,** 1065-1092.

Marengo, J. A., Cavalcanti, I., Satyamurty, P., Trosnikov, I., Nobre, C., Bonatti, J., Camargo, H., Sampaio, G., Sanches, M. Manzi, A. 2003. Assessment of regional seasonal rainfall predictability using the CPTEC/COLA atmospheric GCM. *Climate Dynamics,* 21**,** 459-475.

Messager, C., Gallée, H. Brasseur, O. 2004. Precipitation sensitivity to regional SST in a regional climate simulation during the West African monsoon for two dry years. *Climate Dynamics,* 22**,** 249-266.

Miller, B. I. 1958. On the maximum intensity of hurricanes. *Journal of Meteorology,* 15**,** 184-195.

Minnett, P. J., Evans, R., Kearns, E. Brown, O. Sea-surface temperature measured by the Moderate Resolution Imaging Spectroradiometer (MODIS). Geoscience and Remote Sensing Symposium, 2002. IGARSS'02. 2002 IEEE International, 2002. IEEE, 1177-1179.

Mlawer, E. J., Taubman, S. J., Brown, P. D., Iacono, M. J. Clough, S. A. 1997. Radiative transfer for inhomogeneous atmospheres: RRTM, a validated correlated-k model for the longwave. *Journal of Geophysical Research: Atmospheres,* 102**,** 16663-16682.

Nayak, R. K. 2006. *Coupling between North Indian Ocean and monsoon.* Ph.D

Palmen, E. 1948. On the formation and structure of tropical hurricanes. *Geophysica,* 3**,** 26-38.

Raju, A., Parekh, A. Gnanaseelan, C. 2014. Evolution of vertical moist thermodynamic structure associated with the Indian summer monsoon 2010 in a regional climate model. *Pure and Applied Geophysics,* 171**,** 1499-1518.

Rao, D. V. B., Ashok, K. Yamagata, T. 2004. A numerical simulation study of the Indian summer monsoon of 1994 using NCAR MM5. *Journal of Meteorological Society, Japan,* 82**,** 1755-1775.

Samala, B. K., Banerjee, S., Kaginalkar, A. Dalvi, M. 2013. Study of the Indian summer monsoon using WRF–ROMS regional coupled model simulations. *Atmospheric Science Letters,* 14**,** 20-27.

Shahi, N. R., Agarwal, N., Mathur, A. K. Sarkar, A. 2011. Atmospheric correction for sea surface temperature retrieval from single thermal channel radiometer data onboard Kalpana satellite. *Journal of earth system science,* 120**,** 337-345.

Shetye, S. R., Gouveia, A. D., Shankar, D., Shenoi, S. S. C., Vinayachandran, P. N., Sundar, D., Michael, G. S. Nampoothiri, G. 1996. Hydrography and circulation in the western Bay of Bengal during the northeast monsoon. *Journal of Geophysical Research: Oceans,* 101**,** 14011-14025.

Skamarock, W. C. Klemp, J. B. 2008. A time-split nonhydrostatic atmospheric model for weather research and forecasting applications. *Journal of Computational Physics,* 227**,** 3465-3485.

Stark, J. D., Donlon, C. J., Martin, M. J. McCulloch, M. E. OSTIA: An operational, high resolution, real time, global sea surface temperature analysis system. Oceans 2007-Europe, 2007. IEEE, 1-4.

Uma, R. Selvaraj, S. R. 2012. Lyapunov Exponents and predictability of cyclonic disturbances over the North Indian Ocean. *International Journal of Current Research,* 4**,** 165-168.

Wick, G. A., Emery, W. J., Kantha, L. H. Schlüssel, P. 1996. The behavior of the bulk-skin sea surface temperature difference under varying wind speed and heat flux. *Journal of Physical Oceanography,* 26**,** 1969-1988.

Wicker, L. J. Skamarock, W. C. 2002. Time-splitting methods for elastic models using forward time schemes. *Monthly weather review,* 130**,** 2088-2097.

Yamamoto, M. Hirose, N. 2009. Regional atmospheric simulation of monthly precipitation using high-resolution SST obtained from an ocean assimilation

model: Application to the wintertime Japan Sea. *Monthly Weather Review,* 137**,** 2164-2174.

Zeng, X., Zhao, M., Dickinson, R. E. He, Y. 1999. A multiyear hourly sea surface skin temperature data set derived from the TOGA TAO bulk temperature and wind speed over the tropical Pacific. *Journal of geophysical research,* 104**,** 1525-1536.

Zhang, Y., Li, T., Wang, B. Wu, G. 2002. Onset of the Summer Monsoon over the Indochina Peninsula: Climatology and Interannual Variations. *Journal of Climate,* 15**,** 3206-3221.

Figure Captions:

Figure 1. Temporal variation of Sea Surface Temperature (SST) measured from Buoy (Longitude: 90° E, Latitude:1.5° N) with NCEP SST and GHRSST during 01 May 2010 to 30 September 2010.

Figure 2. (a) Spatial distribution of mean temperature at 850 hPa from NCEP final analysis, RMSD (equation 1) in WVMR forecasts at 850 hPa from (b) CNT and (c) GSE experiments when compared with NCEP final analysis, and (d) forecast impact (FI; equation 2) in WVMR for GSE experiments compared to CNT experiments during 01 June 2010 to 30 September 2010.

Figure 3. Same as Figure 2 but for water vapor mixing ratio (WVMR) at 850 hPa.

Figure 4. Same as Figure 2 but for surface (at 10 meter) wind speed.

Figure 5. Time-series plot of domain average value of (a) surface (2-meter air) temperature, (b) surface (2-meter air) relative humidity, and (c) surface (10-meter air) wind speed forecasts from CNT and GSE experiments and corresponding NCEP final analysis (FNL) during 01 June 2010 to 30 September 2010.

Figure 6. Spatial distribution of mean daily rainfall from (a) TRMM 3B42 merged-rainfall product, and corresponding mean daily rainfall forecasts from (b) CNT and (c) GSE experiments, and (d) forecast impact in rainfall forecasts for GSE experiments compared to CNT experiments during 01 June 2010 to 30 September 2010.

Figure 7. (a) Equitable Threat Score (ETS) and (b) bias score (BS) for the WRF model predicted daily accumulated rainfall at different rainfall thresholds.

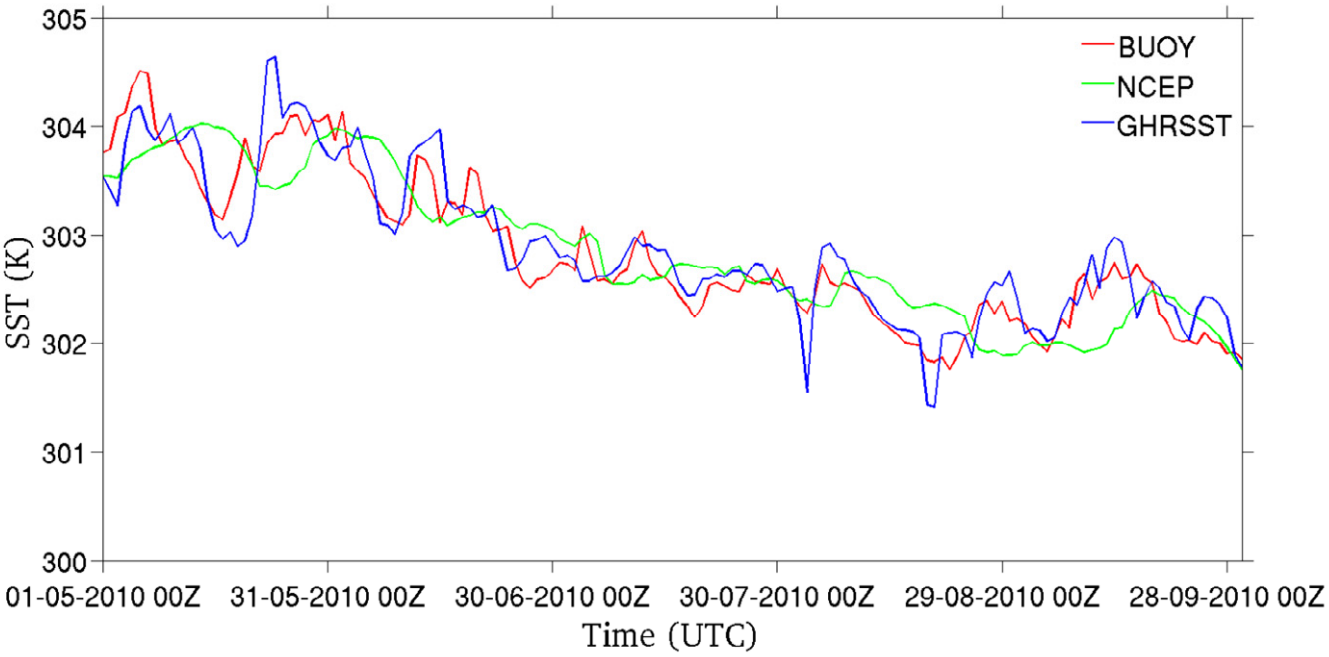

Figure 1. Temporal variation of Sea Surface Temperature (SST) measured from Buoy (Longitude: 90° E, Latitude:1.5° N) with NCEP SST and GHRSST during 01 May 2010 to 30 September 2010.

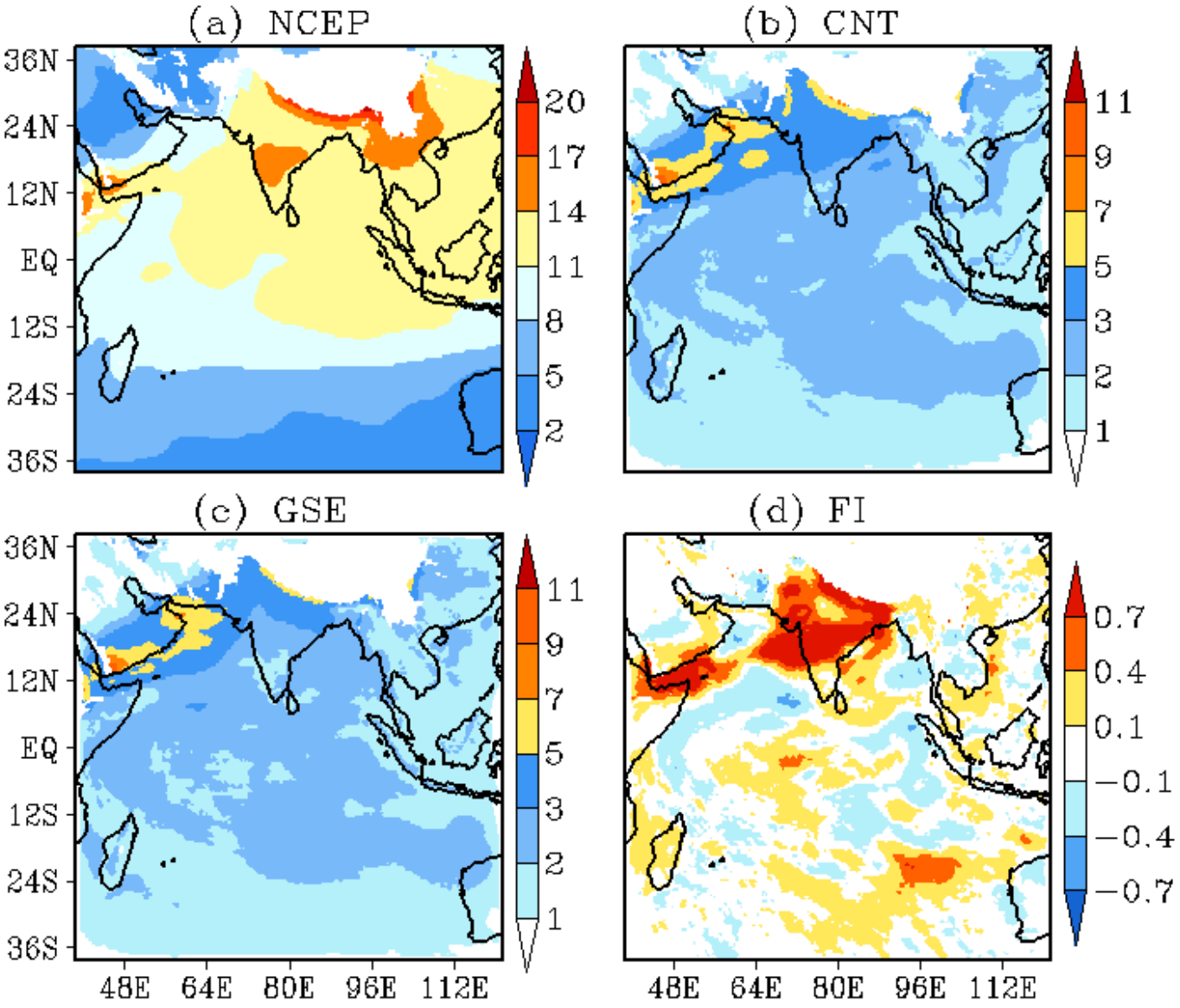

Figure 2. (a) Spatial distribution of mean temperature at 850 hPa from NCEP final analysis, RMSD (equation 1) in WVMR forecasts at 850 hPa from (b) CNT and (c) GSE experiments when compared with NCEP final analysis, and (d) forecast impact (FI; equation 2) in WVMR for GSE experiments compared to CNT experiments during 01 June 2010 to 30 September 2010.

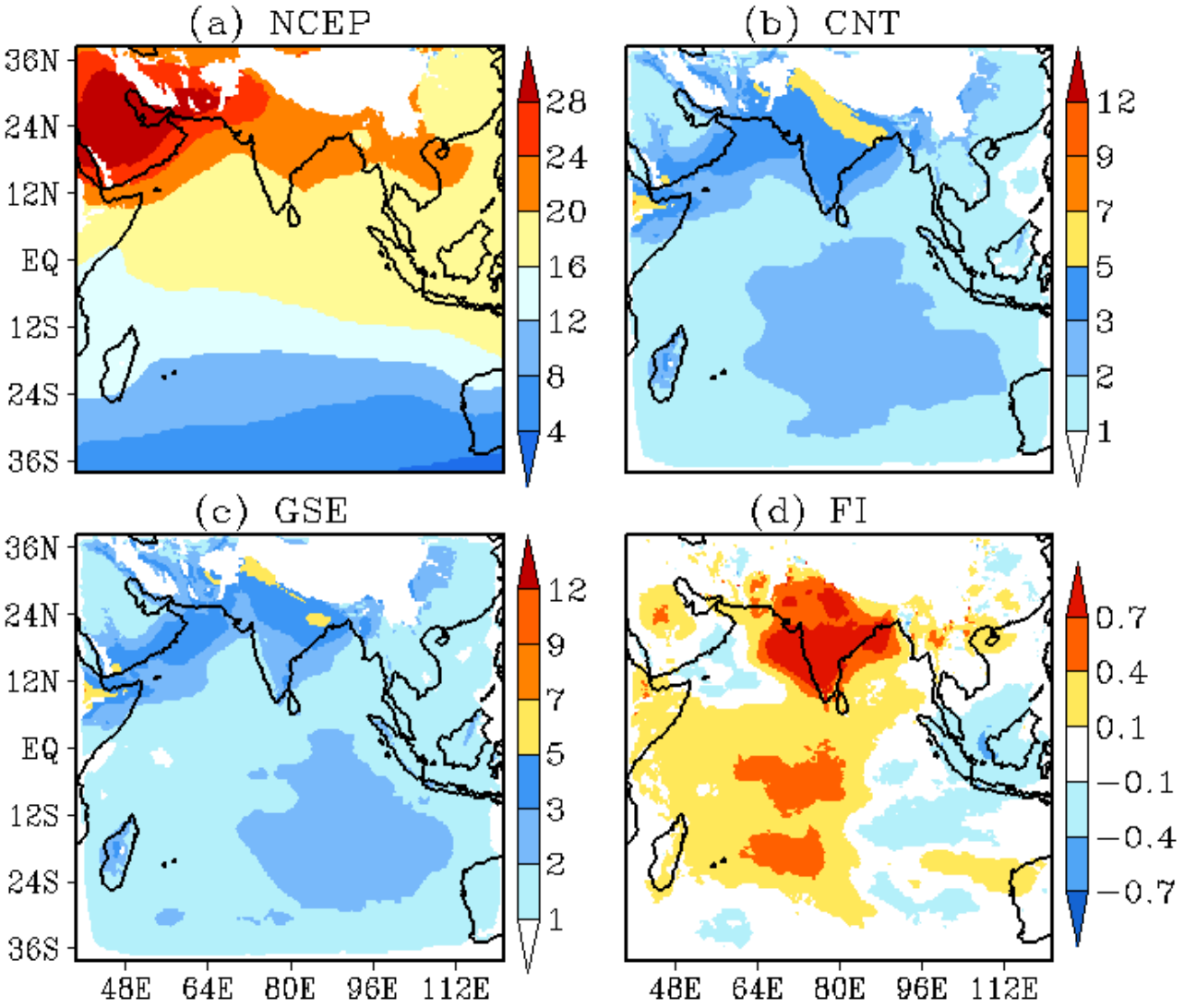

Figure 3. Same as Figure 2 but for water vapor mixing ratio (WVMR) at 850 hPa.

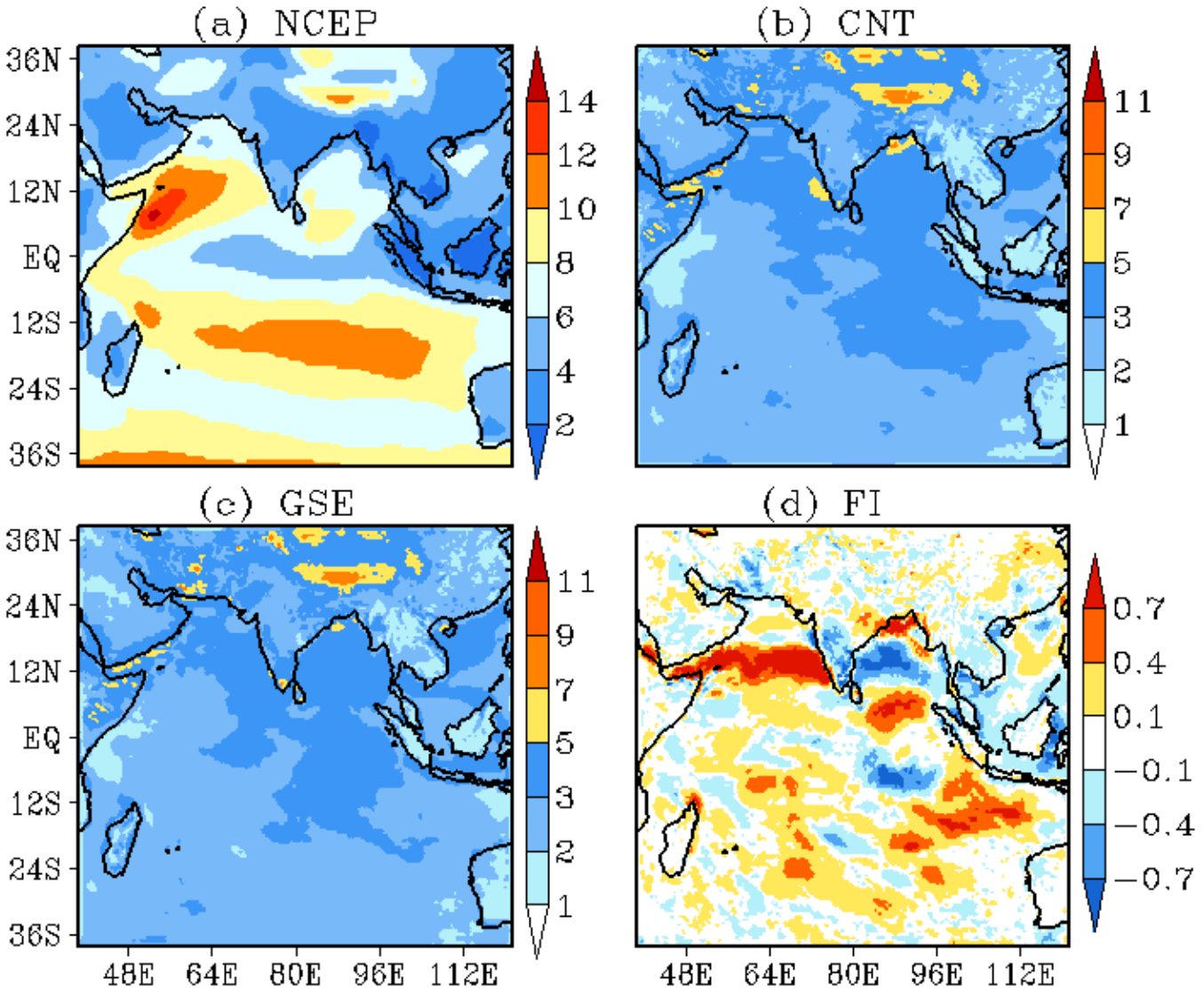

Figure 4. Same as Figure 2 but for surface (at 10 meter) wind speed.

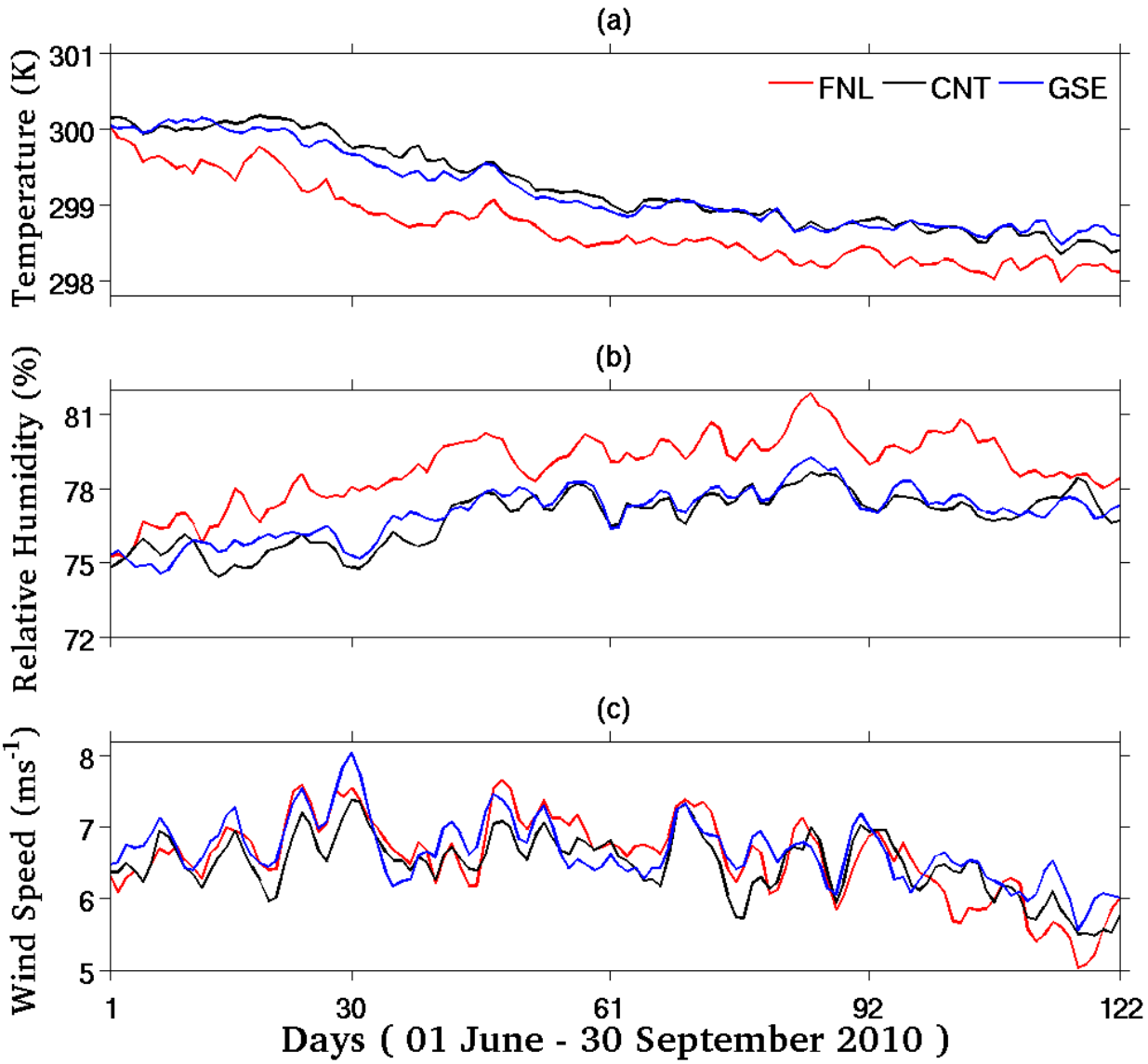

Figure 5. Time-series plot of domain average value of (a) surface (2-meter air) temperature, (b) surface (2-meter air) relative humidity, and (c) surface (10-meter air) wind speed forecasts from CNT and GSE experiments and corresponding NCEP final analysis (FNL) during 01 June 2010 to 30 September 2010.

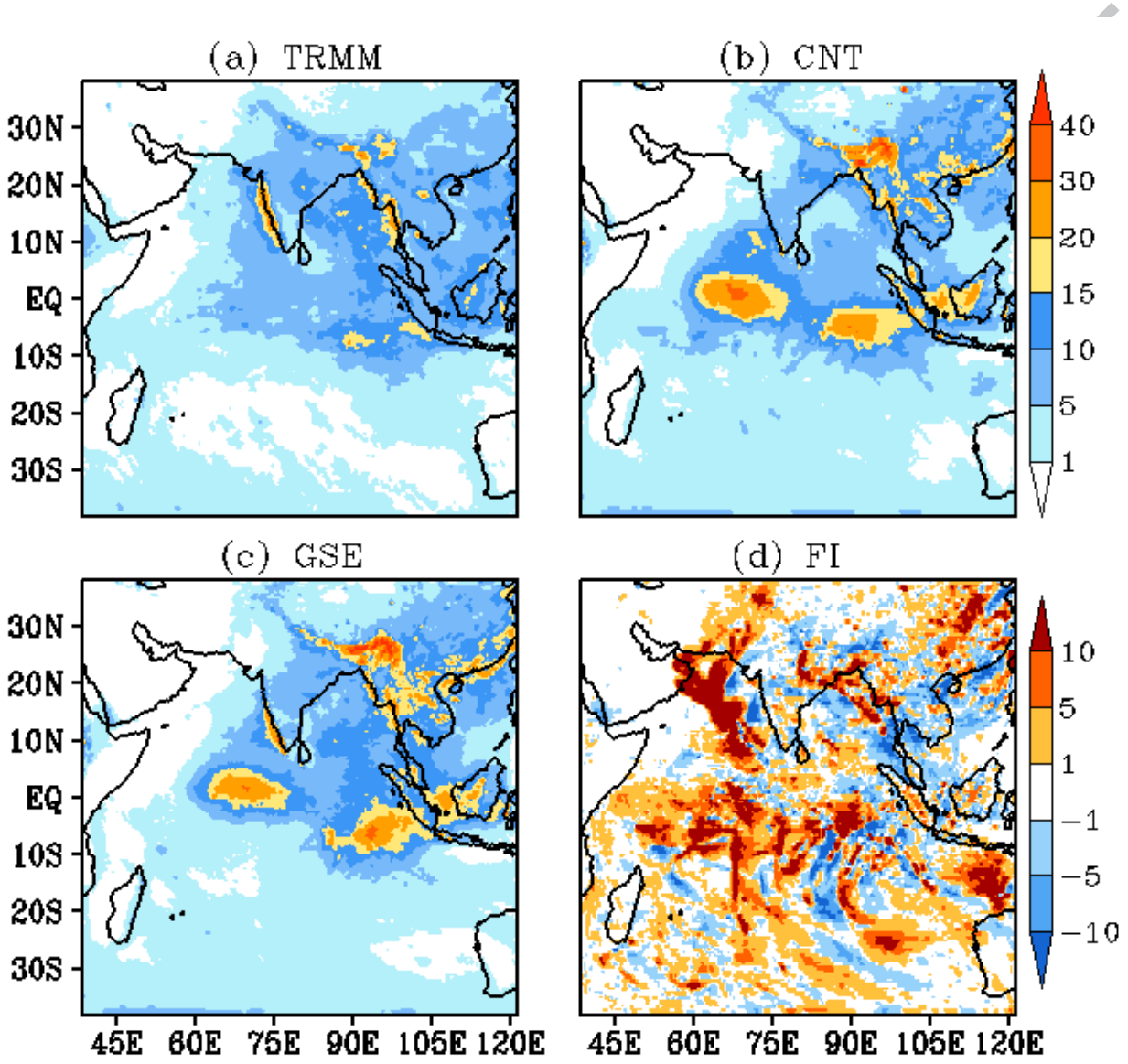

Figure 6. Spatial distribution of mean daily rainfall from (a) TRMM 3B42 merged-rainfall product, and corresponding mean daily rainfall forecasts from (b) CNT and (c) GSE experiments, and (d) forecast impact in rainfall forecasts for GSE experiments compared to CNT experiments during 01 June 2010 to 30 September 2010.

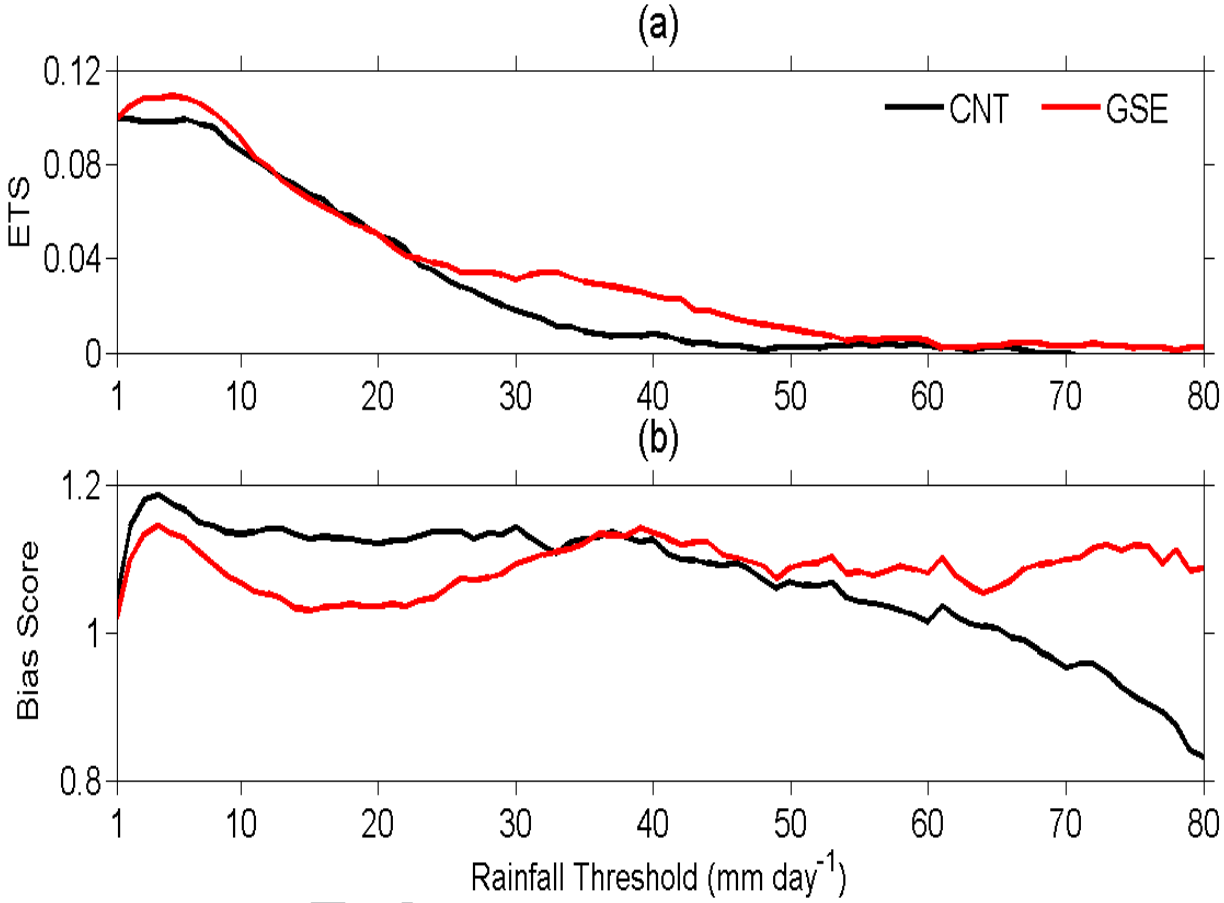

Figure 7. Equitable Threat Score (ETS) and (b) bias score (BS) for the WRF model predicted daily accumulated rainfall at different rainfall thresholds.